

# In-plane quartz-enhanced photoacoustic spectroscopy

Cite as: Appl. Phys. Lett. **116**, 061101 (2020); <https://doi.org/10.1063/1.5142330>

Submitted: 12 December 2019 . Accepted: 01 February 2020 . Published Online: 10 February 2020

Yufei Ma , Shunda Qiao, Pietro Patimisco, Angelo Sampaolo, Yao Wang, Frank K. Tittel, and Vincenzo Spagnolo 



View Online



Export Citation



CrossMark

Lock-in Amplifiers  
Find out more today



 Zurich Instruments

AIP  
Publishing

# In-plane quartz-enhanced photoacoustic spectroscopy

Cite as: Appl. Phys. Lett. **116**, 061101 (2020); doi: [10.1063/1.5142330](https://doi.org/10.1063/1.5142330)

Submitted: 12 December 2019 · Accepted: 1 February 2020 ·

Published Online: 10 February 2020



View Online



Export Citation



CrossMark

Yufei Ma,<sup>1,a)</sup>  Shunda Qiao,<sup>1</sup> Pietro Patimisco,<sup>2,3</sup> Angelo Sampaolo,<sup>2,3</sup> Yao Wang,<sup>1</sup> Frank K. Tittel,<sup>4</sup> and Vincenzo Spagnolo<sup>2,3</sup> 

## AFFILIATIONS

<sup>1</sup>National Key Laboratory of Science and Technology on Tunable Laser, Harbin Institute of Technology, Harbin 150001, China

<sup>2</sup>PolySense Lab–Dipartimento Interateneo di Fisica, University and Politecnico of Bari, Via Amendola 173, Bari 70126, Italy

<sup>3</sup>State Key Laboratory of Quantum Optics and Quantum Optics Devices, Institute of Laser Spectroscopy, Shanxi University, Taiyuan 030006, China

<sup>4</sup>Department of Electrical and Computer Engineering, Rice University, 6100 Main Street, Houston, Texas 77005, USA

<sup>a)</sup>Electronic mail: [mayufei@hit.edu.cn](mailto:mayufei@hit.edu.cn)

## ABSTRACT

An optical gas sensing technique based on in-plane quartz-enhanced photoacoustic spectroscopy (IP-QEPAS) is reported. In IP-QEPAS, the laser beam is aligned in the plane of the quartz tuning fork (QTF) to increase the interaction area between the acoustic wavefront and the QTF. A custom T-shaped QTF with a prong length of 9.4 mm and a resonance frequency of 9.38 kHz was designed and employed in the IP-QEPAS sensor. For comparison, the traditional QEPAS sensor in which the laser beam is perpendicular to the QTF plane (PP-QEPAS) is investigated with the same operating conditions. Theoretical calculations of strain and displacement of the QTF prong were performed to support the advantage of using the IP-QEPAS technique. By selecting water vapor as the gas target, the IP-QEPAS sensor results in a signal more than 40 times higher than that measured with the PP-QEPAS configuration, confirming the potential of this approach.

Published under license by AIP Publishing. <https://doi.org/10.1063/1.5142330>

Due to the merits of high detection sensitivity and selectivity, cost advantage, non-invasiveness, and *in situ* detection,<sup>1,2</sup> optical gas sensing techniques fill a distinct gap between compact, low-cost gas sensors with poor detection sensitivity, such as electrochemical sensors and costly instruments, providing a high sensitivity level, such as gas chromatographs or mass spectrometer systems. Optical gas sensors are widely exploited in numerous fields such as atmospheric monitoring,<sup>3</sup> combustion diagnostics,<sup>4</sup> life sciences,<sup>5</sup> and early fire detection.<sup>6</sup>

Among the most sensitive optical detection techniques, quartz-enhanced photoacoustic spectroscopy (QEPAS) can offer a high degree of robustness and compactness.<sup>7</sup> Due to the photoacoustic effect, acoustic waves are generated when the modulated light is absorbed by the target gas. A quartz tuning fork (QTF) is used as a sensitive acoustic wave transducer to detect sound waves within the gas. The two prongs of the QTF are deflected by the acoustic wavefronts incident on them. Sequentially, electrical charges are produced through the direct piezoelectric effect occurring in quartz and collected by the gold contact pattern deposited on the QTF surfaces.<sup>8,9</sup> In QEPAS, the photoacoustic response depends on the relaxation rates of the target analyte with respect to the gas matrix and the QTF

resonance frequency  $f_0$ , which must be chosen to achieve the highest radiation-to-sound conversion efficiency.<sup>10</sup> Based on the typical values of relaxation rates, the optimum QTF  $f_0$  for photoacoustic detection spans from a few kHz to 40 kHz.<sup>7,11,12</sup> The usually used QTF has a  $f_0$  value of 32.7 kHz (which is used in watches as a crystal oscillator for timing). According to the Euler–Bernoulli theoretical model,  $f_0$  of the first flexural mode (fundamental) of the QTF is given by<sup>13</sup>

$$f_0 = \frac{1.194^2 \pi W}{8\sqrt{12}L^2} \sqrt{\frac{E}{\rho}} \propto \frac{W}{L^2}, \quad (1)$$

where  $W$  and  $L$  are the width and length of QTF prongs, respectively. Thus, by varying the prong thickness and length, the resonance frequency can be predicted with good precision. Starting from 2013, many custom QTFs were designed specifically for spectroscopic applications by optimizing the geometry and the size of the prongs to: (i) reduce the resonance frequency; (ii) achieve a high the Q-factor; and (iii) enlarge the prong spacing to facilitate laser beam alignment.<sup>13</sup> To obtain  $f_0$  in the kHz-range,  $L$  has to be within the millimeter-range and  $W/L^2$  is chosen to match the desired resonance frequency.

In QEPAS, the laser beam should pass through the gap between the two prongs of the QTF in order to produce a QTF signal. In traditional QEPAS sensing, the laser beam is aligned to be perpendicular to the QTF plane (called “perpendicular plane-QEPAS, abbreviated as PP-QEPAS”)<sup>14–18</sup> as shown in Fig. 1(a). Therefore, the effective region for the acting acoustic wave is limited by the thickness  $T$  of QTF prongs. In this paper, we propose a different approach, in which the collimated laser beam propagates in-plane between the prongs, along the QTF vertical axis, to exploit the full prong length  $L$  as the interacting path length between the exciting source and the target gas molecules [see Fig. 1(b)]. As a result, the interaction between the cylindrical acoustic wave and the internal surface of the prongs should be enhanced. We refer to this method as in-plane quartz-enhanced photoacoustic spectroscopy (IP-QEPAS). An IP-QEPAS sensor was realized, and water vapor in standard air was selected as the target gas species to assess the performance of this proposed configuration.

The QTF employed in this work has prongs with a T-shaped geometry and rectangular grooves carved on their surfaces. With respect to the standard rectangular shape, T-shaping of the prong geometry has been demonstrated to increase the strain field on the prong base, providing in turn an enhancement of the photoacoustic response in terms of the signal-to-noise ratio.<sup>19</sup> Compared to a QTF with a rectangular shape (see Fig. 1),  $f_0$  of the T-shaped QTF is reduced by a few tens of percent, while the resonance Q-factor is not affected. In addition, when rectangular grooves are applied on both surfaces of each prong, the capacitance between the two electrodes increases, resulting in a strong reduction of the electrical resistance (up to 30%), while  $f_0$  is only slightly affected (a few percent). The T-shaped QTF with rectangular grooves carved on both prong sides used in this work is depicted in Fig. 2(a). The QTF prong has a full length of  $L = L_1 + L_2 = 9.4$  mm, a crystal thickness of  $T = 250$   $\mu\text{m}$ , and  $W_1$  and  $W_2$  of 2 mm and 1.4 mm, respectively. The distances  $D_1$  and  $D_2$  between the two prongs are 1 mm and 1.2 mm, respectively. The prong surfaces were carved with 50  $\mu\text{m}$ -deep rectangular grooves.

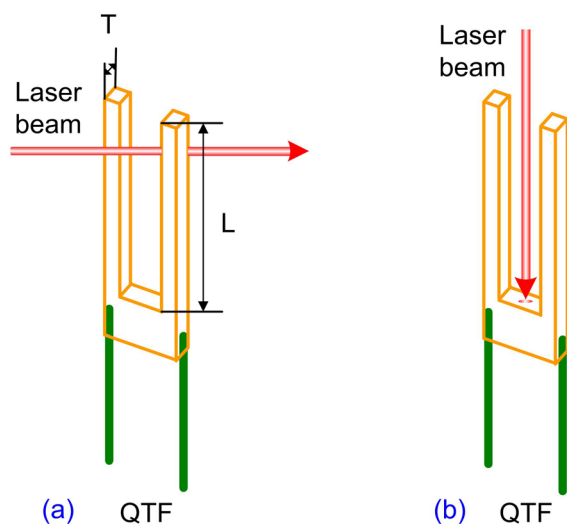


**FIG. 1.** (a) PP-QEPAS configuration. The laser beam (a red arrow) travels perpendicular to the QTF plane. (b) IP-QEPAS configuration. The laser beam travels in the QTF plane.

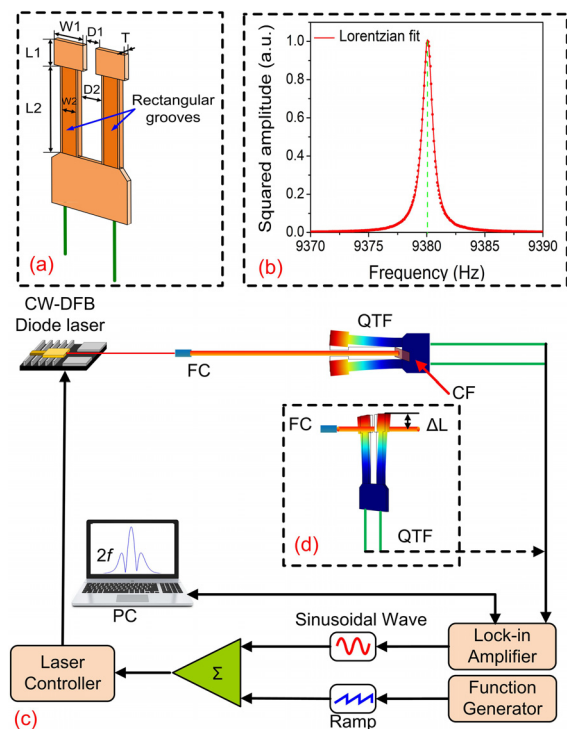


**FIG. 2.** (a) Sketch of a custom T-shaped QTF.  $L_1 = 2.4$  mm;  $L_2 = 7.0$  mm;  $W_1 = 2.0$  mm;  $W_2 = 1.2$  mm;  $D_1 = 1$  mm;  $D_2 = 1.2$  mm;  $T = 250$   $\mu\text{m}$ . (b) Resonance curve (red dots) of a T-shaped QTF at atmospheric pressure. The red solid line is the best fit by using a Lorentzian function. The dotted green line indicates the peak position of the resonance curve. (c) Schematic configuration of the IP-QEPAS sensor system. (d) Schematic configuration of the PP-QEPAS sensor system. FC: fiber collimator; QTF: quartz tuning fork; CF: copper film; PC: personal computer;  $\Delta L$ : the distance between the top of the QTF prongs and the diode laser beam.

The resonance frequency and the quality factor were measured by using the inverse piezoelectric effect. Electrical excitation was provided to the QTF by applying a sinusoidal voltage signal spanning a wide frequency range. The generated QTF piezo-current is fed to a current-to-voltage converter based on a transimpedance operational amplifier. The output voltage as a function of the excitation voltage signal is depicted in Fig. 2(b). By fitting the QTF resonance curve with a Lorentzian function,  $f_0$  and a detection bandwidth  $\Delta f$  were estimated to be 9.38 kHz and 1.06 Hz, respectively. Therefore, based on the equation  $Q = f_0/\Delta f$ , the Q factor was calculated to be 8850, which is comparable to that usually measured for standard 32.7 kHz-QTFs, although the resonance frequency is reduced by a factor of three.

The experimental configuration of an IP-QEPAS sensor is shown in Fig. 2(c). A continuous wave (CW), distributed feedback (DFB), fiber-coupled diode laser with an emitting wavelength of 1.395  $\mu\text{m}$  was employed as the excitation source. The output beam of the CW-DFB diode laser was collimated by using a fiber collimator (FC, Thorlabs, model 50–1310A-APC) with a divergence angle of 0.25°. To avoid any photothermal effect,<sup>20–22</sup> a copper film tilted by an angle of  $\sim 45^\circ$  with respect to the QTF plane was placed nearby the bottom of the QTF prongs (not touching the QTF surface) to deflect the laser beam out of the QTF plane. Water vapor ( $\text{H}_2\text{O}$ ) was chosen as the target analyte.

A  $\text{H}_2\text{O}$  absorption line at  $7168.4\text{ cm}^{-1}$  with a line strength of  $1.17 \times 10^{-20}\text{ cm/molecule}$ , free from interference from other molecules in air, was selected.<sup>23</sup> Wavelength modulation spectroscopy (WMS) with second harmonic ( $2f$ ) demodulation was employed as the detection scheme. Modulation of the laser wavelength was achieved by dithering the current driver with a sinusoidal wave with a frequency of  $f = f_0/2$ . A ramp with a frequency of 20 mHz was added to the laser current driver to scan the wavelength emission across the absorption line. At the  $\text{H}_2\text{O}$  absorption line peak, the CW-DFB diode laser reached an output power of  $\sim 13\text{ mW}$ . A lock-in amplifier (Zurich Instruments, model MFLI) was used to demodulate the  $2f$ -QEPAS signal. The bandwidth and the filter roll-off of the lock-in amplifier were 690 mHz and 24 dB/oct, respectively.

In order to compare with the traditional QEPAS sensor, the PP-QEPAS was investigated initially, whose experimental configuration is shown in Fig. 2(d). Standard air containing 0.83%  $\text{H}_2\text{O}$  in air was used as the target gas mixture. The laser current modulation amplitude giving the highest  $2f$ -QEPAS peak related to water vapor absorption at atmospheric pressure was identified, keeping fixed the distance [ $\Delta L$ , see Fig. 2(b)] between the top of QTF prongs and the diode laser beam at 0.8 mm. The optimum current modulation amplitude was 14.5 mA, corresponding to a wavelength modulation depth of  $0.45\text{ cm}^{-1}$  as shown in Fig. 3(a). The influence of  $\Delta L$  on the PP-QEPAS signal level was investigated, keeping the modulation depth fixed at its optimum value, and the obtained results are shown in Fig. 3(b). The maximum signal level of the PP-QEPAS sensor was  $3.12\text{ }\mu\text{V}$  measured for a laser beam position of  $\Delta L = 1\text{ mm}$ .

Once the optimum operating conditions for the PP-QEPAS sensor were determined, the strain field and lateral displacement of prongs were simulated for the custom T-shaped QTF for both PP- and IP-QEPAS configurations by using COMSOL Multiphysics software with the finite element method (FEM). Both the acoustics pressure field and the solid mechanics field were adopted. The laser beam was modeled as a cylinder, and the side of the cylinder was set as an acoustic line source. A perfectly matched layer (PLM) was used to reduce the reflections of sound at the boundary. For a PP-QEPAS configuration, the acoustic source was located at  $\Delta L = 1\text{ m}$ . The results of simulation are shown in Figs. 4(a)–4(d). In the PP-QEPAS

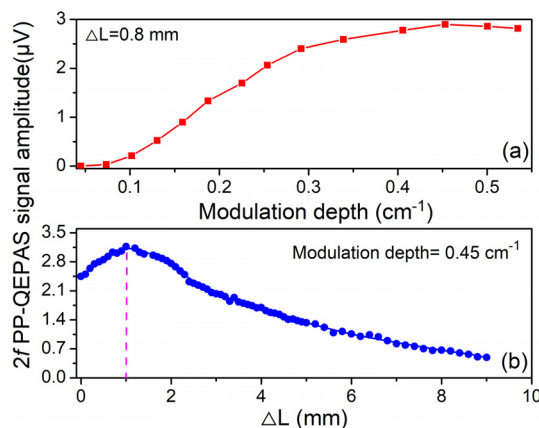


**FIG. 3.**  $2f$  PP-QEPAS signal plotted as a function of modulation depth (a) and plotted as a function of  $\Delta L$  (b).

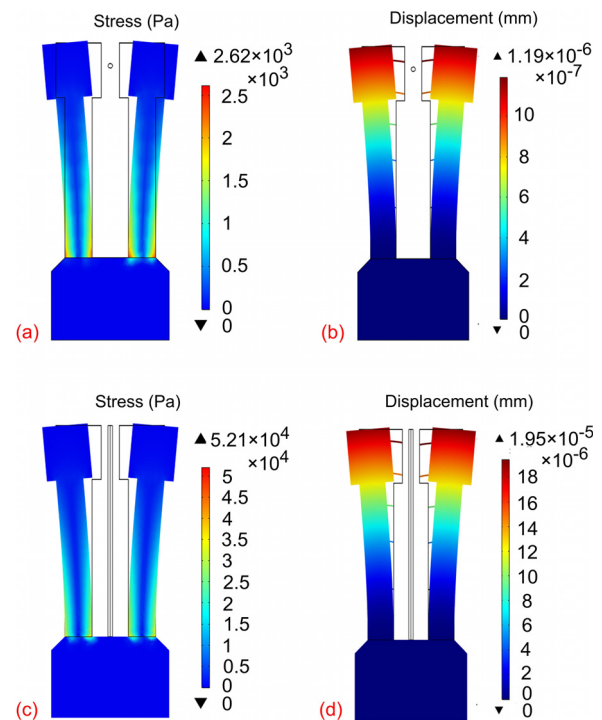


**FIG. 4.** The simulated strain field and lateral displacement of prongs for the T-shaped QTF for different configurations: (a) strain field for the PP-QEPAS sensor; (b) prong displacement for the PP-QEPAS sensor; (c) strain field for the IP-QEPAS sensor; (d) prong displacement for the IP-QEPAS sensor.

configuration, the maximum strain and displacement are  $2.62 \times 10^3\text{ Pa}$  and  $1.19 \times 10^{-6}\text{ mm}$ , respectively. The corresponding values for the IP-QEPAS configuration are  $5.21 \times 10^4\text{ Pa}$  and  $1.95 \times 10^{-5}\text{ mm}$ , respectively, more than one order of magnitude better than those obtained for the PP-QEPAS sensor.

To verify these findings, the performance of the sensor was investigated when implementing the IP-QEPAS configuration with the CW-DFB diode laser beam aligned in the QTF plane. All other experimental conditions are identical to the ones used for the PP-QEPAS configuration. The  $2f$  spectral scan of the  $\text{H}_2\text{O}$  absorption lines is reported in Fig. 5. For comparison, the  $2f$  scan with the PP-QEPAS configuration is also depicted. When the QEPAS sensor is used in the IP-QEPAS configuration, the  $2f$  scan reaches a peak value of  $132.9\text{ }\mu\text{V}$ . Compared to the signal value of  $3.1\text{ }\mu\text{V}$  obtained with the PP-QEPAS configuration, the IP-QEPAS sensor showed a more than 40 times signal enhancement, demonstrating a higher performance with respect to the standard PP QEPAS configuration.

The Allan variance for IP- and PP-QEPAS sensors was investigated when pure nitrogen ( $\text{N}_2$ ) was used as the gas mixture. The measured results are shown in Fig. 6. The Allan variance exhibits a similar behavior for both IP- and PP-QEPAS sensors. Long-term drift for the two sensors appeared only after 200 s, demonstrating the good stability of the sensor system.

In conclusion, the IP-QEPAS configuration was demonstrated as an efficient choice of the standard approach. In the IP-QEPAS technique, the laser beam travels in the QTF plane to increase the

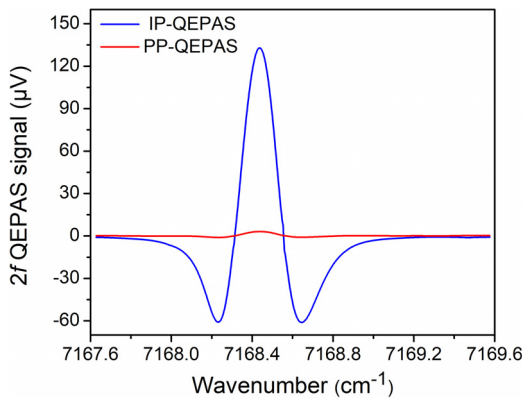


**FIG. 5.** The  $2f$  spectral scan of the selected  $\text{H}_2\text{O}$  absorption line obtained at atmospheric pressure using the IP-QEPAS (blue solid line) and PP-QEPAS (red solid line) sensor by sinusoidally modulating the laser wavelength at  $0.45\text{ cm}^{-1}$ .

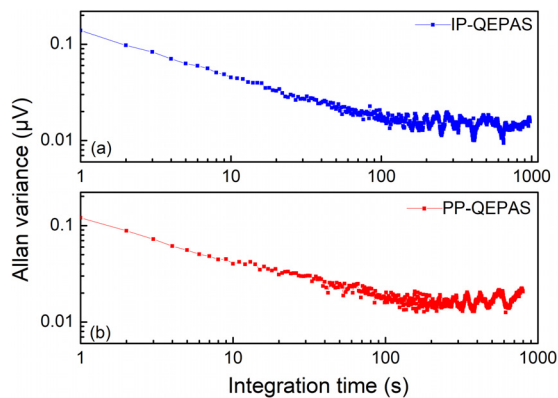


**FIG. 6.** Allan variance for IP- and PP-QEPAS sensors: (a) IP-QEPAS sensor; (b) PP-QEPAS sensor.

interaction area between the generated acoustic wave and QTF. A custom T-shaped QTF with a large prong length of 9.4 mm and a resonance frequency of 9.38 kHz was designed and used to compare the PP- and IP-QEPAS sensors, selecting water vapor in standard air as the target gas species. Finite element modeling was established to simulate the strain and lateral displacement field of prongs of the T-shaped QTF for both IP- and PP-QEPAS configurations. The simulation results support the experimental data observations. At the optimal conditions, the IP-QEPAS sensor recorded a  $2f$  signal of  $132.9\ \mu\text{V}$ , which is  $>40$  times higher than the traditional PP-QEPAS configuration for the same experimental conditions. Allan variance analysis indicated a similar behavior for both the IP- and PP-QEPAS sensors.

This work was supported by the National Natural Science Foundation of China (Grant Nos. 61875047 and 61505041),

Natural Science Foundation of Heilongjiang Province of China (Grant No. YQ2019F006), Fundamental Research Funds for the Central Universities, and Financial Grant from the Heilongjiang Province Postdoctoral Foundation (Grant No. LBH-Q18052). The authors from Dipartimento Interateneo di Fisica di Bari acknowledge the financial support from THORLABS GmbH within the joint-research laboratory PolySense. Frank K. Tittel acknowledges support from the Robert Welch Foundation (Grant No. C0586).

## REFERENCES

- <sup>1</sup>K. Krzempek, G. Dudzik, and K. Abramski, *Opt. Express* **26**, 28861 (2018).
- <sup>2</sup>R. Rousseau, Z. Lohgari, M. Bahriz, K. Chamassi, R. Teissier, A. N. Baranov, and A. Vicet, *Opt. Express* **27**, 7435 (2019).
- <sup>3</sup>L. Tao, K. Sun, M. A. Khan, D. J. Miller, and M. A. Zondlo, *Opt. Express* **20**, 28106 (2012).
- <sup>4</sup>W. Ren, A. Farooq, D. F. Davidson, and R. K. Hanson, *Appl. Phys. B* **107**, 849 (2012).
- <sup>5</sup>T. Milde, M. Hoppe, H. Tatenguem, M. Mordmüller, J. O’Gorman, U. Willer, W. Schade, and J. Sacher, *Appl. Opt.* **57**, C120 (2018).
- <sup>6</sup>J. L. Bradshaw, J. D. Bruno, K. M. Lascola, R. P. Leavitt, J. T. Pham, F. J. Towner, D. M. Sonnenfroh, and K. R. Parameswaran, *Proc. SPIE* **8032**, 80320D (2011).
- <sup>7</sup>Y. F. Ma, *Appl. Sci.* **8**, 1822 (2018).
- <sup>8</sup>H. M. Yi, R. Maamary, X. M. Gao, M. W. Sigrist, E. Fertein, and W. D. Chen, *Appl. Phys. Lett.* **106**, 101109 (2015).
- <sup>9</sup>M. Mordmüller, M. Köhring, W. Schade, and U. Willer, *Appl. Phys. B* **119**, 111 (2015).
- <sup>10</sup>M. Duquesnoy, G. Aoust, J. M. Melkonian, R. Lévy, M. Raybaut, and A. Godard, *Sensors* **19**, 1362 (2019).
- <sup>11</sup>J. Hayden, B. Baumgartner, J. P. Waclawek, and B. Lendl, *Appl. Phys. B* **125**, 159 (2019).
- <sup>12</sup>Y. F. Ma, Y. He, L. G. Zhang, X. Yu, J. B. Zhang, R. Sun, and F. K. Tittel, *Appl. Phys. Lett.* **110**, 031107 (2017).
- <sup>13</sup>P. Patimisco, S. Borri, A. Sampaolo, H. E. Beere, D. A. Ritchie, M. S. Vitiello, G. Scamarcio, and V. Spagnolo, *Analyst* **139**, 2079 (2014).
- <sup>14</sup>Z. L. Li, Z. Wang, Y. Qi, W. Jin, and W. Ren, *Sens. Actuators B: Chem.* **248**, 1023 (2017).
- <sup>15</sup>J. P. Waclawek, H. Moser, and B. Lendl, *Opt. Express* **24**, 6559 (2016).
- <sup>16</sup>S. Gray, A. P. Liu, F. Xie, and C. Zah, *Opt. Express* **18**, 23353 (2010).
- <sup>17</sup>M. Jahjah, S. Belahsene, L. Nähle, M. Fischer, J. Koeth, Y. Rouillard, and A. Vicet, *Opt. Lett.* **37**, 2502 (2012).
- <sup>18</sup>M. Mordmueller, W. Schade, and U. Willer, *Appl. Phys. B* **123**, 224 (2017).
- <sup>19</sup>P. Patimisco, A. Sampaolo, M. Giglio, S. Dello Russo, V. Mackowiak, H. Rossmadl, A. Cable, F. K. Tittel, and V. Spagnolo, *Opt. Express* **27**, 1401 (2019).
- <sup>20</sup>Y. F. Ma, Y. He, Y. Tong, X. Yu, and F. K. Tittel, *Opt. Express* **26**, 32103 (2018).
- <sup>21</sup>Y. He, Y. F. Ma, Y. Tong, X. Yu, and F. K. Tittel, *Opt. Lett.* **44**, 1904 (2019).
- <sup>22</sup>Y. F. Ma, Y. He, P. Patimisco, A. Sampaolo, S. D. Qiao, X. Yu, F. K. Tittel, and V. Spagnolo, *Appl. Phys. Lett.* **116**, 011103 (2020).
- <sup>23</sup>I. E. Gordon, L. S. Rothman, C. Hill, R. V. Kochanov, Y. Tan, P. F. Bernath, M. Birk, V. Boudon, A. Campargue, K. V. Chance, B. J. Drouin, J. M. Flaud, R. R. Gamache, J. T. Hodges, D. Jacquemart, V. I. Perevalov, A. Perrin, K. P. Shine, M.-A. H. Smith, J. Tennyson, G. C. Toon, H. Tran, V. G. Tyuterev, A. Barbe, A. G. Császár, V. M. Devi, T. Furtenbacher, J. J. Harrison, J.-M. Hartmann, A. Jolly, T. J. Johnson, T. Karman, I. Kleiner, A. A. Kyuberis, J. Loos, O. M. Lyulin, S. T. Massie, S. N. Mikhailenko, N. Moazzen-Ahmadi, H. S. P. Müller, O. V. Naumenko, A. V. Nikitin, O. L. Polyansky, M. Rey, M. Rotger, S. W. Sharpe, K. Sung, E. Starikova, S. A. Tashkun, J. Van der Auwera, G. Wagner, J. Wilzewski, P. Wcislo, S. Yu, and E. J. Zak, *J. Quant. Spectrosc. Radiat. Transf.* **203**, 3 (2017).